

CFD-based Computations of Flexible Helicopter Blades for Stability Analysis

Guru P. Guruswamy *
NASA Advanced Supercomputing Division
Ames Research Center, Moffett Field, CA

Abstract

As a collaborative effort among government aerospace research laboratories, an advanced version of a widely used computational fluid dynamics code, OVERFLOW2.1z, was recently released. This latest version includes additions to model multiple flexible, rotating blades. This paper describes how the OVERFLOW code is applied to improve the accuracy of airload computations from the linear lifting line theory that uses displacements from the beam model. In the case used, data transfers required at every revolution are managed through a Unix-based script that runs jobs on large supercluster computers. Results are demonstrated for the 4-bladed UH-60A helicopter, deviations of computed data from flight data are evaluated, and Fourier analysis post-processings suitable for aeroelastic stability computations are performed. Use of airload data for flutter speed computations needed for stability analysis is demonstrated for a typical section of a blade.

Introduction

Accurate aeroelastic computations of helicopter rotor blades involve use of high-fidelity fluids and structures models. The flows are often dominated by shocks waves, blade-vortex interactions and flow separation, and need the use of 3-D Navier-Stokes equations [1]. The primary aeroelastic characteristics of a helicopter rotor blade without accounting for multi-body dynamics can be modeled using beam modes [2].

Several 3-D Navier-Stokes based computational fluid dynamics (CFD) codes are in use today. OVERFLOW, one of the popular CFD codes for rotorcraft applications, has been extensively applied for rigid configurations to-date [3,4]. Of recent OVERFLOW is applied for aeroelasticity by coupling with computational structural dynamics (CSD) methods [2]. FUN3D [5] is another advanced CFD code based on unstructured grid methodology for rotorcraft applications. OVERFLOW uses overset structured grids to model the flow field. Efforts are in progress to add advanced aeroelastic capability to OVERFLOW. Recently, a beam finite-element-based structures [6] was added for isolated blades with a single grid and was demonstrated for cases that do not need trimming. In collaboration with U.S Army engineers [7], NASA added the multi-block-dynamic-deforming grid capability to the latest version of the code, OVERFLOW 2.1z, to compute accurate airloads using the prescribed aeroelastic motions of multiple blades for steady flight [8]. In this effort, OVERFLOW 2.1z solutions are applied to correct the airloads computed from linear aerodynamics based comprehensive analysis (CA) code CAMRAD [9] to improve the accuracy of aeroelastic responses. CAMRAD, which is similar to UMARC [10] and RCAS [11], computes the airloads using lifting-line theory [12], utilizing the displacements from the beam model of the rotor blade.

* Sr. Scientist, Applied Modeling and Simulation Branch, AIAA Associate Fellow

This paper describes computations made using OVERFLOW 2.1z. The prescribed structural deformation data for each revolution is computed using CAMRAD. A Unix script is employed to facilitate the data transfer between OVERFLOW and CAMRAD. Results are demonstrated for a UH-60A helicopter [13] blade. The quality of the results is assessed by computing deviations from measured flight-test data. Fourier analysis is employed to compare data with flight tests. Use of computed data for computing flutter boundary is demonstrated for a typical section of a blade.

Approach

Accurate computations of airloads for the UH-60A rotorcraft in forward flight require trim solutions [14]. The current state-of-the art to compute trim is based on lifting-line solutions tuned with measured thrust forces [7]. Trim solutions exclusively using CFD loads have yet to be developed. In this effort, trim parameters are computed using CAMRAD, which solves the harmonic Hamiltonian equations to give solutions only at the end of each revolution. On the other hand, OVERFLOW is based on a time marching scheme. In order to utilize the trim solutions from CAMRAD, airloads from OVERFLOW are computed at the end of every revolution and applied to correct the airloads of CAMRAD, which in turn are used for computing the aeroelastic displacements. The structural displacements are computed using the beam finite-element solver in CAMRAD. This approach, known as loose coupling (LC), is described step-by-step in the next paragraph.

First, a solution in the form of blade displacement data (known as the motion file for OVERFLOW) is obtained from CAMRAD using flight parameters. The linear lifting-line theory, along with free wake model, is used to compute this initial estimate of motion data from the beam model in CAMRAD. Assuming steady forward flight, this full-revolution motion data, defined to be the same for all blades, is used as a prescribed motion for OVERFLOW. Using the required time step, computations are made for one revolution and aerodynamic forces are computed. These CFD-based aerodynamic loads are used to correct aerodynamic forces in CAMRAD, and a new motion data file with superimposed trim corrections is computed. The new motion data file is used as a prescribed motion in OVERFLOW to compute corrected aerodynamic forces. The CAMRAD/ OVERFLOW computations and data corrections are repeated until the results are converged. Convergence of results is established first by increasing the number of OVERFLOW/CAMRAD iterations and then by increasing the number of time steps per revolution in OVERFLOW.

Figure 1 shows a flow diagram of the OVERFLOW/CAMRAD data exchange process. A Unix shell script [15] is used to facilitate the data exchanges between OVERFLOW and CAMRAD. OVERFLOW is run on Pleiades supercomputer at the NASA advanced supercomputing center facility at Ames Research Center [16] using portable batch system (PBS) [17] with Message Passing Interface (MPI) [18]. CAMRAD is run on a front end Linux node.

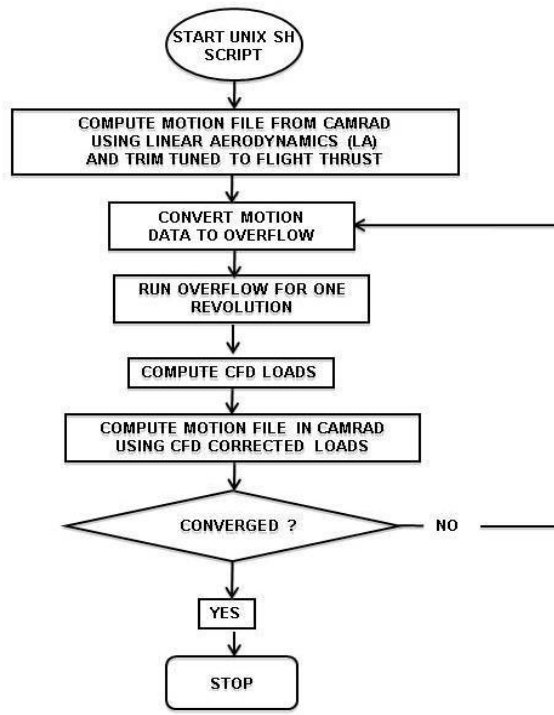


Fig 1. OVERFLOW/CAMRAD data exchange process.

Results

Validation for UH-60A Helicopter Blade System

The 4-bladed UH-60A helicopter, with its extensive set of flight data [13], is selected for demonstrating the latest version (2.1z) of OVERFLOW to correct the airloads and, in turn, aeroelastic displacements computed from CAMRAD. Only the rotor blades are modeled. Each blade has a radius of 322 inches and a chord of 20.76 inches with a swept tip at 92.9% radial station. A 5-million-point overset grid, with 1.9 million near-blade grid points, is selected. All four blades are modeled using 12 overset grid blocks with three blocks for each blade. The three blocks associated with each blade include cap grids at the root and tip sections, as well as a blade grid. The blade surface is represented by a total of 7462 grid points. A portion of the blade geometry and grid near the tip are shown in Figure 2. The high-speed test case C8534 [13], which corresponds to a free-stream Mach number of 0.236 with an advance ratio of 0.37 and a tip Mach number of 0.642 while blades are rotating at a speed of 4.3 Hz, is selected for demonstration.

All computations are made time accurately by using a constant time step in OVERFLOW. First, computations are started with 1440 steps per revolution and CFD/CSD (computational structural dynamics) data exchanges are repeated until the results are converged. Convergence is monitored by tracking the normal force at 86.5% radial station, when the first blade is at 120 degrees azimuth. It required about 25 CFD corrections for convergence. This calculation is repeated by increasing the number of steps per revolution (NSPR) in increments of 1440. Figure 3 shows convergence plots for increasing the NSPR. Results converge at about NSPR = 7200. This is verified by using NSRP = 8640, which produced a result nearly identical with the NSPR = 7200 result.



Fig. 2 A portion of 4-bladed UH-60 rotor grid near blade tip.

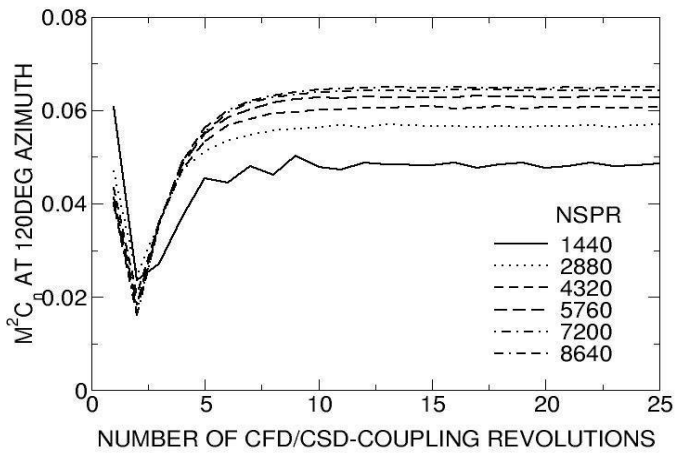


Fig. 3. Convergence of normal force at 86.5% radial station for the first blade.

Plots of computed and flight sectional normal force C_n and pitching moment C_m at 86.5% radial station are shown in figures 4 and 5, respectively. The comparisons are favorable.

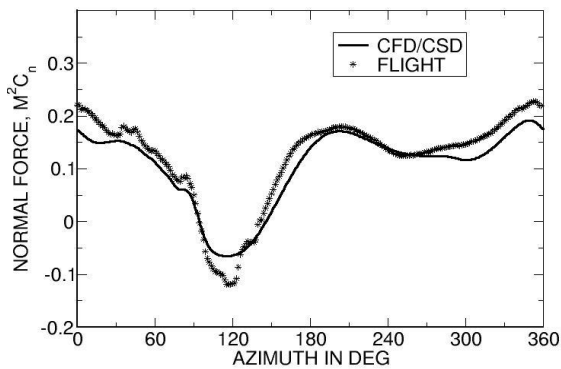


Fig. 4 Comparison of normal force with flight data at a radial station of 86.5% span for the C8534 case of UH-60A rotor.

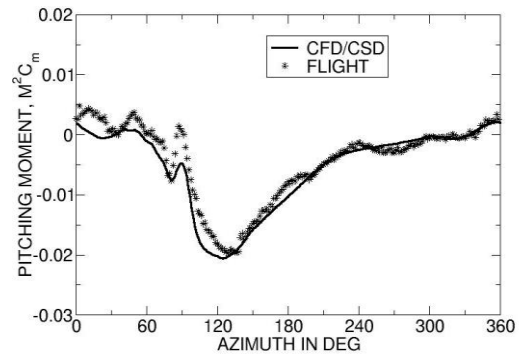


Fig. 5 Comparison of pitching moment with flight data at radial station of 86.5% span for the C8534 case of UH-60A rotor.

Based on the procedure discussed in Ref. 19, deviations of computed C_n and C_m from flight data [13] are calculated. First, a measured value and corresponding azimuth is selected from flight data from figures 4 and 5. The computed force value corresponding to the selected flight azimuth is extracted and its deviation from flight force value is calculated. The plots of these deviations are shown in figures 6 and 7 for C_n and C_m , respectively. All computed values are within 10% of the measured data except for four values that go beyond 10% for C_m . The average deviations are 3.51% and 3.81% for C_n and C_m , respectively. These values are less than the corresponding average deviations, 4.1% and 4.7%, reported in Ref. 19 based on a survey of results taken from the Literature.

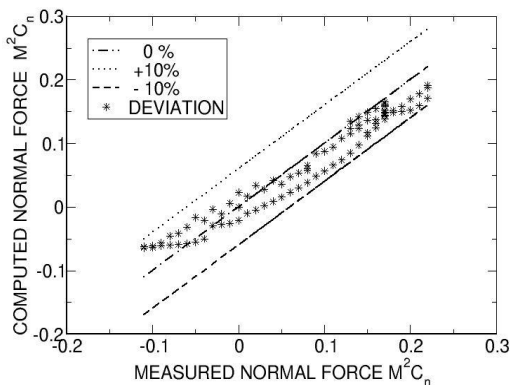


Fig 6. Deviation of computed normal force coefficient for the C8534 flight case of UH-60A rotor system

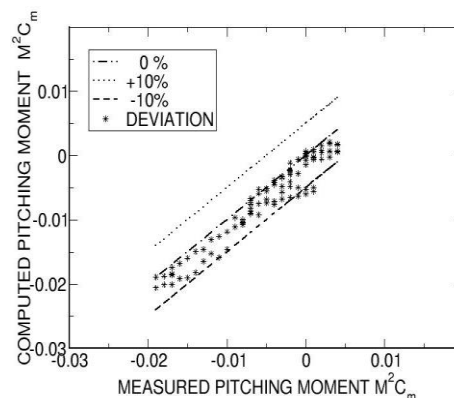


Fig. 7 Deviation of computed pitching moment coefficient for the C8534 flight case of UH-60A rotor system.

Fourier Transformations for Aeroelastic Stability Analysis

The aerodynamic forces computed using OVERFLOW need to be converted to Fourier quantities for use in aeroelastic stability analysis [20]. The deviations shown in figures 6 and 7 provide information only about the magnitude of the airloads. For aeroelastic stability analysis, both magnitude and phase angles play an important role. Fourier analysis [21] also determines the deviations of phase angles from measured data.

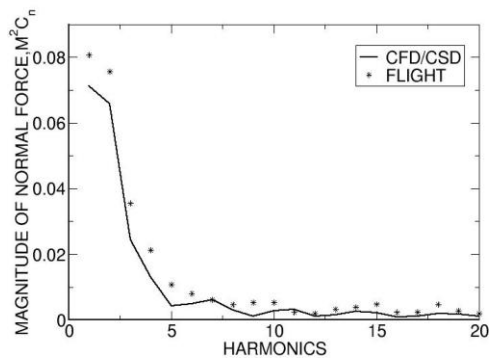


Fig. 8 Comparison of normal force magnitudes at a radial station of 86.5% span for the C8534 case of UH-60A rotor system.

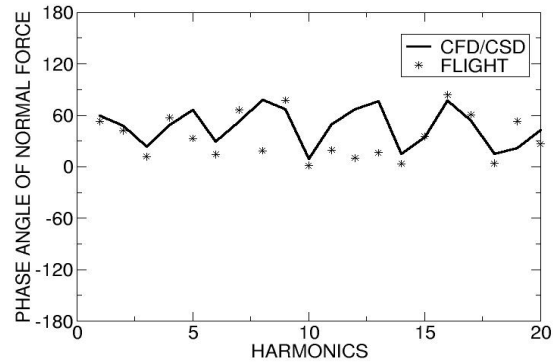


Fig. 9 Comparison of normal force phase angles at a radial station of 86.5% span for the C8534 case UH-60A rotor system.

Fourier transformations [21] are applied to the airloads computed from OVERFLOW. Magnitudes and phase angles with respect to the azimuth of the first blade are computed for 20 harmonics. Figure 8 shows the comparison between computed and flight normal force magnitude at $r/R = 0.865$. The values of magnitude become small after the 9th harmonic.

Comparison between computed and measured data is good for the magnitude of all 20 harmonics. Figure 9 shows corresponding plots for phase angles. The differences between computed and measured phase angles are significant after the 7th harmonic. These differences can be attributed to lack of time-accurate couplings between the OVERFLOW and CAMRAD computations, as well as smaller magnitude of the loads. Figure 10 shows the corresponding comparison of phase angle scaled by the ratio of current magnitude to the magnitude of the first harmonic. This plot shows a good comparison for all harmonics.

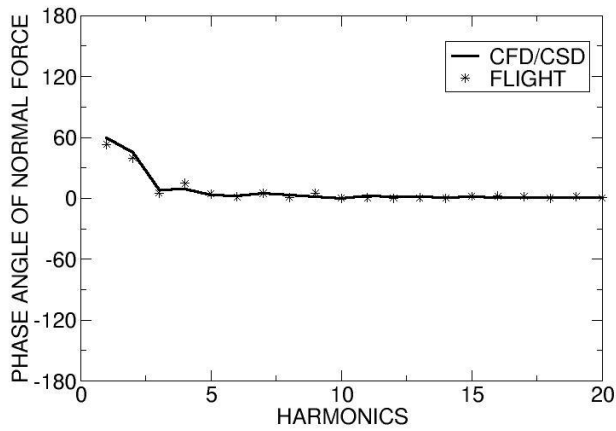


Fig. 10 Comparison of scaled phase angles of normal force at a radial station of 86.5% span for the C8534 case of UH-60A rotor system.

Figure 11 shows a comparison between computed and flight pitching moment magnitudes at $r/R = 0.865$. The pitching moment magnitude becomes small for harmonics higher than about 6. Comparison between computed and measured data is good for all 20 harmonics, except for some discrepancies around the 5th harmonic.

Figure 12 shows the plot of computed and measured phase angles for the pitching moment. The differences between computed and measured phase angles are more significant after the 3rd harmonic. This may be due to low amplitude and lack of time-accuracy in the LC approach. Figure 13 shows the phase angle, scaled by the ratio of the current magnitude to the magnitude of the first harmonic. The scaled values show good comparison for all harmonics.

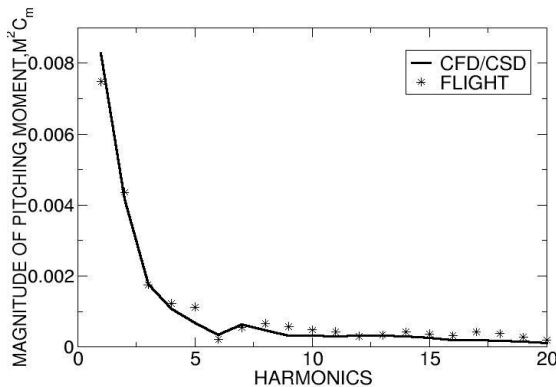


Fig. 11 Comparison of pitching moment magnitudes at a radial station of 86.5% span for the C8534 case of UH-60A rotor system.

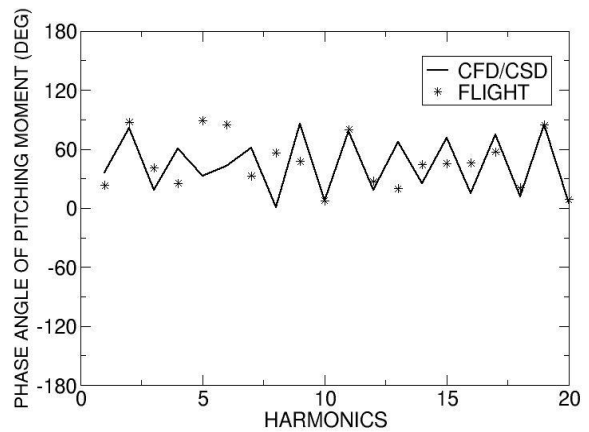


Fig. 12 Comparison of pitching moment phase angles at a radial station of 86.5% span for the C8534 case of UH-60A rotor system.

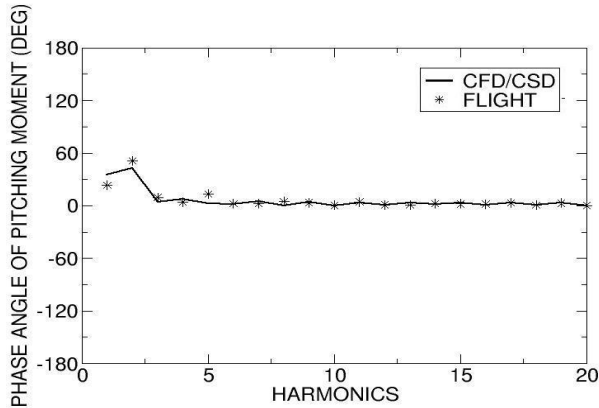


Fig. 13 Comparison of scaled phase angles of pitching moment at a radial station of 86.5% span for the C8534 case of UH-60A rotor system.

From results shown in figures 10 and 13 for normal force and pitching moment of the C8534 case, phase angles of higher harmonics may not have significant contribution on stability computations since the magnitudes are small.

Demonstration for Computing Stability Boundary

The data to compute flutter speeds is not available in the public domain for the UH-60A rotor. As a result, use of computed airloads for calculating flutter speeds is demonstrated for a rotor blade with NACA64A010 airfoil section, and an aspect ratio of 16.

Computations are made for hover conditions. This isolated single blade is modeled using a grid of 150,000 points, adequate for Euler computations in OVERFLOW. For rotor blades, the flutter characteristics are first assessed by computing the flutter speed of the 2-D typical section at a 75% semi-span station [22]. Assuming chordwise rigidity, the 2-D section involves 2 degrees of freedom (DOF), pitch and plunge. The chordwise deformation, which has a secondary effect [22] on flutter speed, is neglected. Computations are made for two rotating speeds such that the local Mach numbers at 75% span station are 0.40 and 0.60. The reduced frequency (defined as $k_r = 4\omega c/3\Omega R$, where ω is the flutter frequency, c is chord length, Ω is rotating speed in radians per second and R is radius of blade) is varied. The rotating speeds corresponding to 0.40 and 0.60 Mach numbers are 33.3 and 50.0 radians per second, respectively. Flutter computations are made using the eigenvalue approach implemented software, TWODOF, reported in Ref. 23. Assuming that the blade is rigid and allowed to twist and flap about the root, computations are made for $k_r = 0.05, 0.10, 0.15$ and 0.20 . Flapping and twisting motions are prescribed.

Computations are made forcing the blade to undergo flapping motion with a tip amplitude of 0.8 chord and a twisting motion with an 1.0 degree amplitude. Three oscillations are required for convergence to a periodic motion at which point the Fourier coefficients are extracted. Figure 14 plots the magnitude of the first harmonic of the lift coefficient, due to twisting motion for both 0.40 and 0.60 Mach numbers. Also shown are

results based on the Kernel function linear theory [24]. Results compare better at $M_\infty = 0.40$ than at $M_\infty = 0.60$. For $M_\infty = 0.60$, differences are more pronounced toward the lower frequencies. It is noted that sectional lifts predicted by both the Euler and the linear theory computations are higher than 6.28, a value based on the quasi-steady ($k_f = 0.0$) linear theory [25].

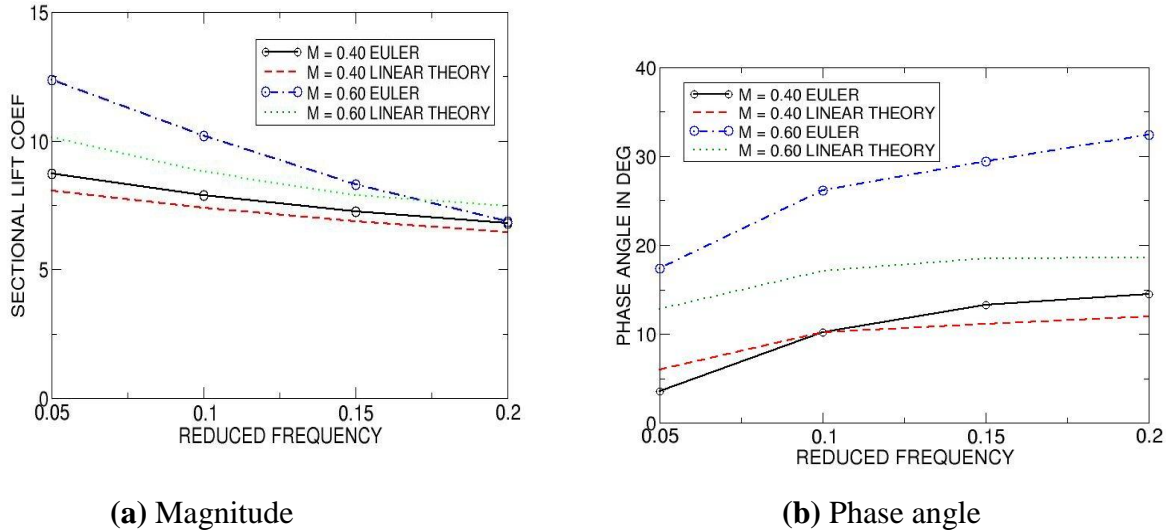


Fig. 14. Magnitude (a) and phase angles (b) of sectional lift coefficients for typical section of NACA64A010 blade in twist motion.

The phase angles of sectional lift forces, with respect to pitching motion computed using the Euler and linear theory equations, are shown in Fig. 15 for $M_\infty = 0.40$ and 0.60 . Euler and linear results are closer to each other for $M_\infty = 0.40$ than for $M_\infty = 0.60$. For $M_\infty = 0.60$, the differences in phase angles increase as k_f increases.

Magnitude and phase angles of moments are extracted similarly to results shown in Figs. 14 (a) and (b), respectively. Based on the magnitude and phase angles of the first harmonic, flutter computations are made using TWODOF. Assuming that the ratio of flapping frequency to torsion frequency is 0.20 and a mass center at mid-chord, then the non-dimensional flutter speed $U_f = (3\Omega R)/(2c\omega_\alpha)$, where ω_α is the torsional frequency in radians per second, is computed. Table I shows the summary of results for both Mach numbers. As expected, the Euler results are closer to the linear theory for $M_\infty = 0.40$ than for $M_\infty = 0.60$.

Table I: Flutter Results

M_∞	LINEAR		EULER	
	U_f	k_f	U_f	k_f
0.40	7.12	0.091	7.20	0.110
0.60	6.01	0.088	5.11	0.092

This section demonstrates the use of newly developed CFD/CSD capabilities for computing the flutter speed. Following the procedures developed for fixed wings [26], the current approach can be extended to a full blade instead of the typical section considered here.

Conclusions

Computations have been made to demonstrate the use of advanced CFD codes for aeroelastic stability analysis of helicopter blades. Loose coupling via Unix scripting works efficiently in transferring data between a high-fidelity CFD code and a low-fidelity CSD code. Accounting for phase angles using Fourier analysis gives better insight into the results than does just considering amplitudes. The CFD corrections to the comprehensive code significantly improves the quality of results. Based on a typical section of a blade, it is shown that post-processed CFD data can be directly utilized in computing the flutter speeds needed for stability analysis. Procedures developed and demonstrated here can be extended for computing the flutter boundary of a full blade.

Acknowledgements

The author would like to thank Mark Potsdam from US Army for providing grids for CFD modeling. Collaborative efforts of Pieter Buning and Doug Boyd from NASA Langley Research Center in implementing OVERFLOW 2.1z towards aeroelastic computations needed for this paper is appreciated. Special thanks to Dennis Jespersen and Ethan Romander, NASA Ames Research Center, for providing consultations on using superclusters and CAMRAD, respectively. The guidance throughout this effort, particularly in computing the deviations from flight, by Terry Holst, the NASA Subsonic Rotary Wing project's CFD lead, was highly valuable.

References

1. Vadyak, J., Shrewsbury, G. E., Narramore, J. C., Montry, G. and Holst, T., "Navier-Stokes Aerodynamic Simulation of the V-22 Osprey on the Intel Paragon MPP, " Document ID 200200122, NASA Technical Report Server, Computational Aeroscience Workshop, Moffett Field, CA, March 1995.
2. Guruswamy, G.P., "A Modular Approach to Euler/Navier-Stokes-Based Aeroelasticity of Helicopter Rotor Blades," AIAA-2008-2179, 49th AIAA/AHS Structural Dynamics Conf, Chicago, April 2008.
3. Potsdam M., and Pulliam, T. H., "Turbulence Modeling Treatment for Rotocraft Wakes," Presented at AHS Aeromechanics Specialist's Meeting, San Francisco, CA, Jan. 23-25, 2008.
4. Holst, T. and Pulliam, T.H., "Overset Solution Adaptive Grid Approach Applied to Hovering Rotorcraft Flows," AIAA-2009-3519, 27th AIAA Applied Aerodynamics Conference, San Antonio, Texas, June 2009.

5. Biedron B. and Thomas, J., "Recent Enhancements to the FUN3D flow solver for Moving Mesh Applications," AIAA-2009-1360, June 2009.
6. Guruswamy, G.P., "Computational-Fluid-Dynamics and Computational-Structural-Dynamics Based Time-Accurate Aeroelasticity of Helicopter Blades," *Jl of Aircraft*, Vol. 47, No. 3, May-June 2010, pp 858-863.
7. Potsdam, M., Yeo, H. and Johnson, W., "Rotor Airloads Using Loose Aerodynamic /Structural Coupling," American Helicopter Society 60th Annual Form, Baltimore, MD, June 2004.
8. Boyd, D. D., "HART-II Acoustic Predictions using a Coupled CFD/CSD methods," American Helicopter Society 65th Annual Forum, Grapevine Texas, May 2009.
9. Johnson, W., "Rotorcraft Aerodynamic Models for a Comprehensive Analysis," American Helicopter Society, 54th Annual Form, Washing ton D. C, May 1998.
10. Datta, A., and Chopra, I., "Validation and Understanding of UH-60A Vibratory Loads in Steady Level Flight," *Journal of the American Helicopter Society*, Vol. 49, (3), July 2004, pp. 271-287.
11. "RCAS Theory Manual, Version 2.0," Technical Report USAMCOM/AFDD TR 02-A-005, US Army Aviation and Missile Command, Moffett Field, CA, June 2000.
12. Gessow, M., "The Aerodynamics of the Forward Flight" *Aerodynamics of the Helicopter*, Fedrick Ungar Publishing, Co, New York, 1967, pp. 180-216.
13. Kufeld, R. M., Balough, D. L., Cross, J. L., Studebaker, K.F., Jenninson, C. D. and Bousman, W. G., "Flight Testing of the UH-60A Airloads Aircraft," American Helicopter Society, 50th Annual Forum, Washington DC, May 1994.
14. Peters, D. A. and Barwey, D., "A general theory of rotorcraft trim," *Mathematical Problems in Engineering*, Volume 2 (1996), Issue 1, pp. 1-34.
15. Robbins, A., Beebe, N. H. F, *Classic Shell Scripting*, O'Reilly Media Inc, 2005, Sebastopol, CA.
16. Guruswamy, G. P, "Large-Scale Computations for Stability Analysis of Launch Vehicles Using Cluster Computers," AIAA 2010-2954, 52nd AIAA/AHS/ Structural Dynamics and Materials conference, Orlando, FL, April, 2010.
17. Stanzione D., "LSF/PBS Scripting Nuts and Bolts," *Cluster World*, Vol. 2 No 7, July 2004.
18. Groop, W., Lusk, E., and Skjellum, A., *Using MPI - Portable Parallel Programming with the Message Passing Interface*, Scientific and Engineering Computing Series. 1999, the MIT Press, Cambridge, Massachusetts.

19. Holst, T.L., Lee-Rausch, M., Biedron, R. T, Guruswamy, G.P., and Kreeger, R. E., "Chapter-4 Computational Fluid Dynamics, A Status of NASA Rotorcraft Research," edited by Yamauchi G. K. and Young, L. A., NASA/TP-2009215369, Sept. 2009, pp. 149-192.
20. Krodkiewski, J.M., " Stabilization of Motion of Helicopter Blades Using Delayed Feedback- Modeling, Computer Simulation and Experimental Verification," *Journal of Sound and Vibration*, (2000) 234(4) pp. 591-610.
21. Kreyszig, E, "Fourier Analysis", *Advanced Engineering Mathematics*, John Wiley & Sons, Inc., Hoboken, NJ, 1976, pp. 478- 529.
22. Bielava, R. L., "Unsteady Aerodynamics and Flutter," *Rotary Wing Structural Dynamics and Aeroelasticity*, AIAA Education Series, Washington D.C.,1992. pp. 379-454.
23. Guruswamy, P. and Yang, T.Y., "Aeroelastic Time Response of Thin Airfoils, " *International Journal of Computers and Fluids*, Vol. 9, No. 4, 1981, pp. 409-425.
24. Bland, S., "Development of Kernel-Function Aerodynamics for Comparison with Time-Dependent Finite Difference Methods ," NASA TM-82283, 1982.
25. Bisplinghoff, R. L., Ashley, H. and Halfman, R. L. "Thin Airfoils Oscillating in Incompressible Flow," *Aeroelasticity*, Addison-Wesley Publishing Company, Menlo Park California, 1955, pp. 278-279.
26. Guruswamy, G. P., "User's Guide for ENSAERO-A Multidisciplinary Program for Fluid/Structural/Control Interaction Studies of Wings," NASA TM 108853, Oct 1994.